1
2
3
4
5
6
7
8
9
10
11
12
13
14
15
16
17
18
19
20
21
22
23
24
25
26
27
28
29
30
31
32
33
34
35
36
37
38
39
40
41
42
43
44
45
46
47
48
49
50
51
52
53
54
55
56
57
58
59
60

Efficient Resistive Switching and Spike Rate Dependent Plasticity in a New $CuCrO_2$ Memristor for Plausible Neuromorphic Systems

Pavan Kumar Reddy Boppidi, Bharathwaj Suresh, Ainur Zhussupbekova, Pranab Biswas, Daragh Mullarkey, P Michael Preetam Raj, Igor V Shvets, and Souvik Kundu

Abstract*—In this work, we introduce a new class of *p*-type transparent conductive oxide (TCO) $CuCrO_2$ (150 nm) heterogeneously integrated onto FTO/glass for forming free memristor based neuromorphic applications. The fabricated Al/$CuCrO_2$/FTO memristors demonstrate a reliable bipolar resistive switching with an ON/OFF ratio of 1000. The retention of the device was found to be steady even beyond 10^6 s, which demonstrates its non-volatility. The current-voltage (I-V) characteristics were fitted to evaluate its transport properties and a band-diagram was projected to have a better insight of the device operational principles. To validate the experimental observations, a new model has been developed, and the simulated I-V behavior was analogues to the experimental one. Efforts were then devoted to observe long-term potentiation (LTP) and long-term depression (LTD) utilizing identical but opposite pulses to evaluate the device's efficacy for synaptic applications. The synaptic behavior was well controlled by the pulse (pulse amplitude and width) variations. The conductance change was found to be symmetric and then saturated, which reflects the popular biological Hebbian rules. Finally, a long-term synaptic modulation has been implemented by establishing the spike rate dependent plasticity (SRDP) rule, which is a part of spiking neural networks and advantageous to mimic the brain's capability at low power. All the obtained experimental results were systematically corroborated by neural network simulation. Overall, our approach provides a new road map towards the development of TCO based alternative memristors, which can be employed to mimic the synaptic plasticity for energy-efficient bio-inspired neuromorphic systems and non-Von Neumann computer architectures.

***Index Terms*—Resistive Switching, $CuCrO_2$ Memristors, Synapse, Spike Rate Dependent plasticity.**

I. Introduction

MEMRISTOR is a two-terminal circuit element which can store and process data in terms of its electronic resistance [1]. As compared to the complementary metal-oxide-semiconductor (CMOS) devices, the most significant features responsible for popularity of the memristors are its nanoscale dimensions, low power consumption, high memory density, faster write-read cycles, low-cost and simple fabrication methods [2]. Owing to the above-mentioned merits, efforts have been devoted to study the impact of incorporating memristors for important applications such as non-volatile memory (NVM), neuromorphic computing, digital electronics, and analog electronic system [1], [3], [4]. Recently, the ability of the memristor to perform in-memory computing was beneficial for neuromorphic applications, which received tremendous research interest since the conventional computations are in-efficient owing to the Von Neumann bottleneck [3], [5], [6]. To address neuromorphic systems, CMOS based Spiking Neural Networks (SNNs) have been widely studied. However, due to the problems associated with the scaling limit of CMOS technology, it will be difficult in achieving synapse density similar to that found in the human brain [7]. In this regard, the memristive features such as its analog behavior, plasticity, high packing density, non-volatility, and low power consumption are valuable to mimic the synaptic functionality which performs the weight updates between interconnected neurons [5], [6].

Several researchers have investigated numerous materials such as organic semiconductors [8], perovskite oxides [9], ferroelectrics [2], polymers [10], transition-metal oxides (TMO) [11], transparent-conductive-oxide (TCO) [12], etc. to realize memristive devices. Among these materials, the recent study of TCO thin films has led to the development of simplest geometry-based point contact resistive switching devices with advantages in terms of repeatability, robustness and stacking density [12]. Earlier, researchers have found different *n*-type TCOs such as indium tin oxide (ITO), doped zinc oxide (In:ZnO), metal doped strontium titanate (STO), amorphous indium gallium zinc oxide (IGZO), etc., which established a tremendous commercial success, but achieving *p*-type conductivity in those TCOs is very limited [13]-[16]. Interestingly, all the popular TCOs are made of In, which is not only quite brittle and often cracks on substrates under a low strain when deposited over large areas, but also added up cost due to the increasing In price [13], [14]. Therefore, despite their commercial success, significant efforts have been put to find alternative *p*-type TCO to replace In-rich TCOs, which could also offer *p-n* junction in the transparent electronics sector. Furthermore, the memristors based on *n*-

P.K.R. Boppidi, B. Suresh, P.M.P. Raj, and S. Kundu are with the Dept. of Electrical & Electronics Engineering, BITS-Pilani, Hyderabad Campus, Hyd - 500078, India. (Corresponding author's e-mail: souvikelt@gmail.com or souvik.kundu@hyderabad.bits-pilani.ac.in). A. Zhussupbekova, P. Biswas, D. Mullarkey and I. V. Shvets are with the School of Physics, Trinity College, The University of Dublin, D02PD91 Dublin 2, Ireland.

type TCO materials have been widely celebrated, unfortunately, a very little attention has been paid to develop *p*-type TCO based devices and its neuromorphic systems. To meet the constant demand for developing a new class of TCO, some of the present authors successfully synthesized a novel *p*-type copper chromium oxides ($CuCrO_2$) and reported its structural, conducting and transport properties [13], [14], [17]. Other researchers have also put their efforts to study only the structural or material properties in their synthesized $CuCrO_2$ [15], [18]. The $CuCrO_2$ offers (i) high density of state of 3d M cations (Cr^{3+}) near the valence band maximum, (ii) mixing of chromium and oxygen covalent ions, and (iii) better dopability [15], which make the material suitable for potential resistive switching (RS) device applications since oxygen vacancy plays a pivotal role in realizing the switching process. Moreover, the electrical conductivity of other TCOs is associated to their long range crystalline order, which required higher processing temperature in excess of 600 ºC. Fortunately, $CuCrO_2$ does not require such high temperature processing and crystalline order above the nanoscale range to retain its electrical conductivity [14]. Furthermore, there was no attempt initiated yet to study the memristive or neuromorphic properties of the said material, and this knowledge gap motivates the present authors to perform further investigation to stimulate the diverse TCO electronic sectors.

When neuromorphic systems are concerned, the manipulation of memristive analog characteristics for the synaptic and neuromorphic systems are still underdeveloped [19]. Nevertheless, the important activities such as long-term potentiation (LTP) and long-term depression (LTD) have inspired the development of machine learning applications in different memristor-based neural networks [3]. In our brain, the neurons generate spikes at very low frequency, which ensures that the power consumption is minimal [20], [21]. Based on certain properties of the neuron spikes, the synaptic weight gets varied, and information is encoded. A learning rule defines how the synaptic weight gets varied in a synapse [21]. One such learning rule is called 'spike-timing dependent plasticity' (STDP), wherein the weight of the synapses gets changed depending on the difference in timing between pre- and post-synaptic spikes [3], [22]. Although STDP offers several advantages for use in memristive neural networks, this technique also became well matured and studied by many researchers (including us) without any significant improvement [3], [20], [23], [24]. On the other side, STDP requires spikes that have to be engineered to a particular shape. This increases complexity of the neuron circuit that produces the Pre- and Post-Synaptic spikes. In this context, the other learning rule 'spike rate-dependent plasticity' (SRDP) inspired by biology is rarely studied as a method to change the state of the devices in such memristive neural networks [25]. Chang et. al. simulated the SRDP mechanism by employing phase transition memristors [26]. Despite these foundational advancements, the role of SRDP to implement advanced neural networks is rarely explored on oxide systems [27], [28]. Another shortcoming of STDP is that a pulse delay circuit is required in addition to the pulse generator to yield STDP spikes of appropriate delay. On the other side, SRDP spikes can easily be reproduced as the pulse generator circuit itself generates pulses of the required frequency. Hence demonstrating such behavior in any new materials based memristor is paramount for their utility in efficient neuromorphic computing.

In this work, we propose a synaptic Al/$CuCrO_2$/FTO/Glass memristors and systematically study its effectiveness for neuromorphic applications. To understand its current-voltage (I-V) behavior, a band-diagram has been projected and the obtained electrical results were correlated. To demonstrate the efficacy of the proposed memristor for neuromorphic applications, biological synaptic characteristics LTP and LTD were established. A careful study was initiated to tune the analog or synaptic behaviors through the pulse (amplitude and width) variations, which can be engaged to actualize the learning potentialities in synapse. An attempt has also been made to establish the SRDP learning mechanism for updating synaptic weights. To validate the experimental observations, attempts were consecrated to model the I-V characteristics and perform tests through circuit simulations. A generic methodology of Verilog-A template has been used to model the I-V by adjusting appropriate parameters [29]. The model was also considered to demonstrate the variation of conductance when voltage pulses having different amplitudes and pulse widths were considered.

II. Devices And Experiments

To fabricate the Al/$CuCrO_2$/FTO/glass memristor, firstly, the FTO coated glass of 1 x 1 cm^2 was rinsed using acetone followed by ultra-sonicated in DI water for 5 minutes. The FTO (10 Ω/sq.) was also used as bottom electrode. Copper acetylacetonate and chromium acetylacetonate (acac) were utilized as precursors (owing to their stability in air, and low toxicity), whereas methanol was employed as a solvent for the preparation of $CuCrO_2$ active layer. The precursors of copper acetylacetonate $(acac)_2$ and chromium $acac_2$ were dissolved in methanol (Cr/Cu: 70/30) with overall molarity of 0.03M in order to obtain $CuCrO_2$ solution. The active layer ($CuCrO_2$) was deposited onto the FTO substrate through a simple spray pyrolysis method. The solution of $CuCrO_2$ was sprayed through an air blast nozzle (PNR, model MAD-0331) by utilizing a mixture of compressed air/nitrogen (95%/5%) with a gas flow rate of 1.70 ml/min over heated (360°C) FTO coated glass [13], [17]. Al electrodes with a thickness of 70 nm and a diameter of 0.20 mm were served the purpose for top electrodes, which were patterned on the $CuCrO_2$ layer through the E-beam evaporation unit (HHV, BC-600) in a class 100 cleanroom. Field Emission Scanning Electron Microscopy (FESEM) (Apreo LoVac, Retractable STEM 3 Detector, resolution of 127 eV on Mn-kα) and X-ray Photo-electron Spectroscopy (XPS) (Thermo Scientific K-Alpha) were utilized to examine the surface and interfacial morphologies of the $CuCrO_2$/FTO. Fittings of the obtained XPS spectra were accomplished using a nonlinear least-squares (Gaussian or Lorentzian fitting) technique. At room temperature, the

electrical properties of the fabricated devices were measured using Keysight B2912A source meter. The top electrode Al was biased with respect to the bottom FTO electrode during all the electrical measurements. The device simulation was carried out using the generic Verilog-A model developed by T. Wang and J. Roychowdhury [29]. This model was actualized using the Spectre® simulator under the Cadence® Virtuoso® 6.1.5 Analog Design Environment®. The voltage waveforms to perform the required simulation were obtained by programming scripts in MATLAB® R2015a.

III. Results And Discussion

For XPS analysis, all the binding energies were corrected with reference to the C1s line at 285.12 eV. Fig. 1(a) illustrates the survey spectra of $CuCrO_2$ thin film. The peaks located at 932.19, 577.97, and 531.78 eV were assigned to Cu, Cr, and O, respectively. The core level Cu2p spectrum shown in Fig. 1(b) exhibits two main peaks placed at 932.20 and 951.90 eV representing the $Cu2p_{3/2}$ and $Cu2p_{1/2}$, respectively. The $Cu2p_{3/2}$ main peak was de-convoluted and the obtained two peaks were located at 931.8 and 932.50 eV. The peak found at 932.50 eV indicates the presence of Cu^{1+} and the existence of Cu_2O in the samples. The spin-orbit splitting between binding energies of $Cu2p_{3/2}$ = 932.20 and $Cu2p_{1/2}$ = 951.90 was found to be 19.70 eV, which supports the formation of $CuCrO_2$ phase and its oxidation state of copper to be Cu^{1+} [15], [30]. Fig. 1(c) depicts the Cr2p spectrum where two intense peaks of Cr2p such as $Cr2p_{3/2}$ = 576.40 and $Cr2p_{1/2}$ = 586.20 were observed with the spin-orbit splitting of 9.80 eV, which is in accordance with the Cr^{3+} oxidation state [15], [30].

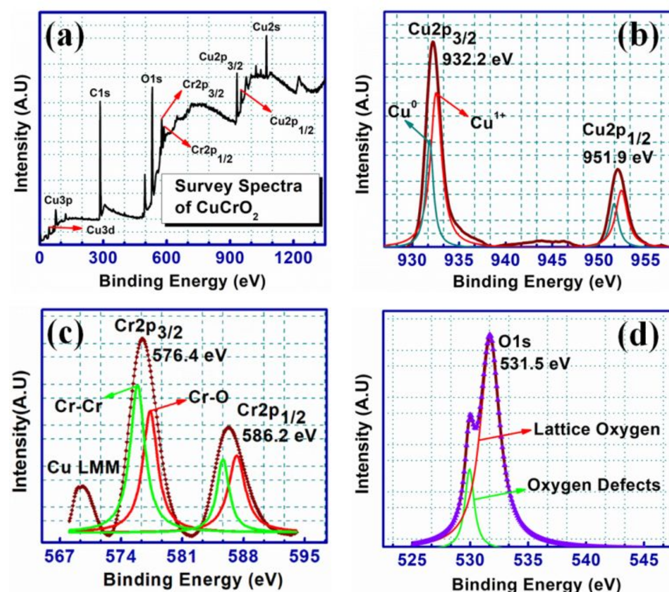

Fig. 1. XPS of $CuCrO_2$ thin film (a) Survey spectrum of $CuCrO_2$, (b) The Cu2p spectra confirms that Cu exists in Cu^0 and Cu^{1+}states, (c) The binding energies of de-convoluted $Cr2p_{3/2}$ show the existence of Cr-Cr and Cr-O bonds with a +3 oxidation state, and (d) The de-convoluted O1s spectra show the signature of oxygen defects and lattice oxygen.

Surprisingly, the Cu Auger peak (Cu LMM) was also observed at 569.40 eV and two oxidation states such as Cu^0 and Cu^{1+} were believed to be the origin for this peak [15], [31]. Therefore, the Auger peak designates the signature of Cu^{1+} in our deposited thin-films. Fig. 1(d) shows the O1s spectra, where the two de-convoluted peaks (located at 529.9 and 531.5 eV) confirm the presence of lattice oxygen and oxygen vacancies. It is noteworthy to mention that these oxygen vacancies can be beneficial for the realization of forming free memristive devices.

Fig. 2(a) displays the FESEM micrograph of the $CuCrO_2$ thin film deposited onto FTO/glass. From the micrograph, it was observed that the film has particles with a spherical shape, which was distributed uniformly throughout the surface. The deposited film was uniform, densely packed and continuous with no voids and pit holes, which eventually prevents charge leakage and may enhance the device performance. In addition, the cross-sectional FESEM image confirms the thickness of the deposited film $CuCrO_2$ onto FTO/glass (shown in the inset of Fig. 2(a)), which was found to be 150 nm. One can also note that there was no cross diffusion from the glass substrate into the active layer, which further confirms the high chemical stability in $CuCrO_2$. To observe the resistive switching in the proposed TCO, a positive voltage was probed on the Al top electrode, and negative voltage to the bottom FTO as shown in Fig. 2(b). In order to record the switching behaviour in the fabricated device, the I-V measurements were recorded by sweeping the voltage from negative to positive. Keysight I-V source measurement unit was used to obtain these characteristics through maintaining the voltage mode as a linear double sweep for the voltage range from – 3 V to + 3 V. As the voltages were swept from 0 to +3V, +3 to 0, 0 to – 3 V and – 3 to 0 V, a pinched hysteresis was observed, which is the expected feature of a memristor. The switching was observed both at positive and negative voltages, confirms the bipolar nature of the device. Fig. 2(c) represents the log (I) *v/s* V plots of the fabricated memristors for 100 cycles. From the I-V characteristics, one can notice that when the voltage was varied from 0 V, there was no significant current variation and it was in the order of ~nA. This indicated that the device was initially in the high resistive switching (HRS) state. However, when the voltage was varied gradually and reached about 2.60 V, the current suddenly gets increased from its HRS state, it is termed as the SET process, in which the device switches from HRS to low resistive switching (LRS) state. Interestingly, when the voltage was swept back from 3 to 0 V, the device retained its LRS state, possesses its non-volatile property. Then the voltage was swept again from 0 towards – 3 V, and the device switches back to HRS from LRS at a voltage of about – 2.80 V, indicating a RESET process. Furthermore, in order to evaluate the repeatability of the fabricated device, the I-V characteristics were tested for 100 cycles. It was observed that there was negligible change in the I-V characteristics of the device with fixed SET and RESET voltages. The inset of Fig. 2(c) displays the endurance property, where the LRS and HRS currents were recorded for 100 cycles. The LRS and HRS exhibit uniform currents (negligible deviation) throughout the measurement. This indicates that the fabricated devices were highly reliable, thanks to the property of the novel $CuCrO_2$ thin films and its stability. High ON/OFF current ratio (~1000 at 0.10 V) obtained from the memristor

also establishes its effectiveness for high-performance NVM

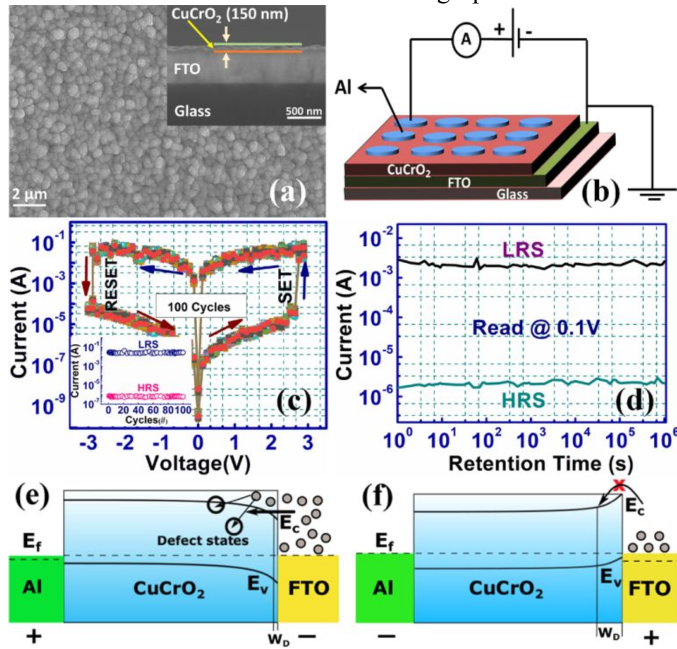

Fig. 2. (a) Surface morphology of deposited $CuCrO_2$. Inset gives an X-sectional SEM micrograph of $CuCrO_2$, FTO, and Glass, (b) Schematic of the fabricated memristive device, (c) Recorded I-V characteristics and endurance (inset) of the fabricated device, (d) Charge retention characteristics of the devices. Band diagrams of $CuCrO_2$/FTO interface (e) Under forward bias, and (f) Under reverse bias.

operation. To further demonstrate its effectiveness for non-volatile memory operation, it is essential to measure the charge retention over a large time period. The same has been performed for the fabricated memristor, which offers stable retention over 10^6 s. During the measurement, the device also maintained a stable ON/OFF ratio of ~1000 as shown in Fig. 2(d), which possesses its robustness for reliable memory operation. To facilitate a better understanding of the resistive switching process, band diagrams with respect to LRS (under forward bias) and HRS (reverse bias) states were projected. The bottom electrode FTO offers its *n*-type nature due to the fact that fluorine-doped in tin oxide results in the generation of free electrons and oxygen vacancies [32], [33]. On the other hand, $CuCrO_2$ was observed to have *p*-type nature (confirmed through Hall measurements and hot probe technique). Hence, a *p-n* junction is created and a depletion layer (W_D) is formed, as shown in Fig. 2(e). Initially, the number of unfilled traps (in this case oxygen vacancies) will be higher than the total injected carriers. Hence, no current can flow, resulting in the HRS or OFF state of the device. When a positive voltage was probed to the top Al electrode of the device as shown in Fig. 2(e), the state changes from HRS to LRS as the voltage gets increased and arrive at SET voltage. In addition, unlike other filamentary based devices, electrons from the bottom electrode (FTO) start getting trapped into the defect states in $CuCrO_2$ and the available traps start to get filled due to band bending at the junction. This results in an increase of electrons at the interface and consequently a decrease in the depleted layer. Hence the device switches from HRS to LRS state [2], [34]. As the carrier concentration of *n*-type FTO is much higher than *p*-type $CuCrO_2$, the barrier is found to be narrower in *n*-type FTO compared to *p*-type $CuCrO_2$. This is also evident from Fig. 2(e) and 2(f), where the depletion width W_D of HRS is larger compared to LRS. Conversely, when a negative voltage was probed on Al, the electrons get de-trapped from the oxygen vacancies and moved back to FTO. At the junction, no further electrons movement is possible from FTO towards $CuCrO_2$ since the band bends upward at the junction and the device moves back to the HRS state (Fig. 2(f)). It is evident that the trapping and de-trapping of electrons in oxygen vacancies occur at opposite voltage polarities, which confirms the bipolar nature of the $CuCrO_2$ device. Thus, the presence of excess charge and oxygen vacancies play a decisive role in the modification of current states in our devices, which is forming free, as it relies on trap assisted SCLC model [34], [35] for operation. As a result, $CuCrO_2$ memristors offer excellent switching properties and can be considered for highly reliable neuromorphic applications. In order to study the switching processes in the proposed memristor, the charge transport phenomena were ascertained through fitting the I-V readings of HRS and LRS in the log-log scale as shown in Fig. 3. This analysis was performed for

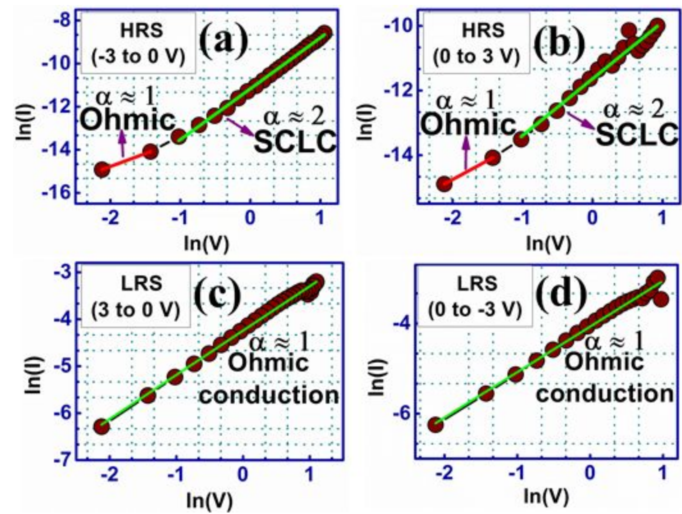

Fig. 3. Study of the charge transport phenomena in the memristors for the cases of (a) –3 V to 0 V HRS, (b) 0 V to 3 V HRS, (c) 3 V to 0 V LRS, and (d) 0 V to –3 V LRS.

both positive and negative voltages. When the voltage was varied from –3 to 0 V (during HRS), the graph in Fig. 3(a) was mapped to space charge limited current (SCLC) and Ohmic conductions as the slope of the linear fit was $\alpha > 2$ and $\alpha = 1$, respectively. Similar situation has also been observed when the voltage was increased from 0 to 3 V (shown in Fig. 3(b)) as $\alpha \approx 2$ for SCLC and $\alpha = 1$ for Ohmic conductions were obtained. At SET voltage ($\approx$ 2.60 V), it was observed that the state of the device was changed from HRS to LRS. When the voltage was brought down from 3 to 0 V, one can notice that the obtained current was changed linearly to the applied voltage since $\alpha \approx 1$, as shown in Fig. 3(c). Importantly, the device retained its LRS state, which was continued for the voltage ranging from 0 to – 3 V as depicted in Fig. 3(d). Thus, the Ohmic conduction was responsible for these cases as shown in Fig. 3(c) and 3(d). This study affirms that the SCLC

was the dominant factor for HRS, whereas the Ohmic charge transport mechanism was responsible during LRS.

In order to realize the artificial synaptic behavior in Al/$CuCrO_2$/FTO memristors, a model was used to mimic the electrical characteristics. As memristive devices have NVM property, there is a need to include a state variable $s(t)$ to govern the relation between current $i(t)$ and voltage $v(t)$. Hence, the relation between $i(t)$ and $v(t)$ is in the form: [29]

$$i(t) = f(v(t), s(t)) \quad (1)$$

As the state of the memristor is also a dynamic entity, the change $s(t)$ is given by: [29]

$$\frac{d}{dt}s(t) = g(v(t),s(t)) \quad (2)$$

Functions f and g that satisfy (1) and (2) can be used to model the switching behavior in memristors. In this work, we consider the same functions as [29].

$$f(v(t),s(t)) = \frac{v(t)}{R}.(tanh\,(k.s(t)) + 1) \quad (3)$$

$$g(v(t), s(t)) = \frac{1}{\tau}.(v(t) - s^3(t) + s(t)) \quad (4)$$

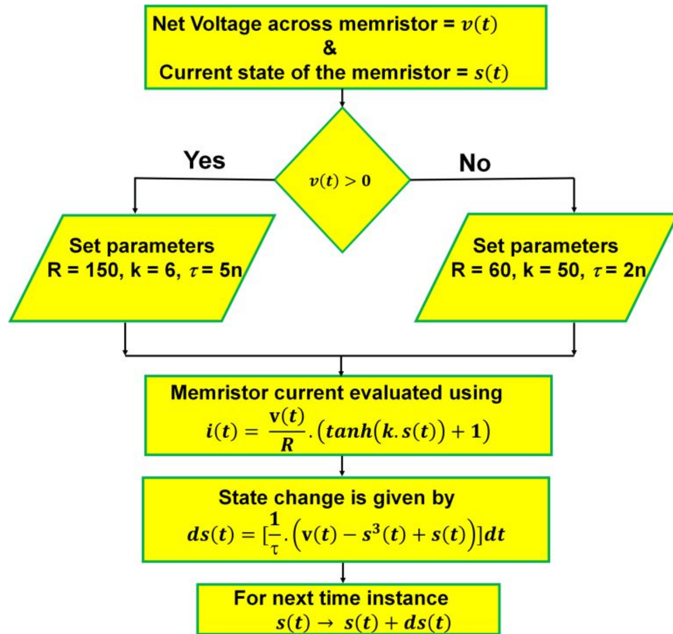

Fig. 4. Flow chart of the memristive state programming.

The parameters R, k, and τ determine the nature of the hysteresis loop obtained through simulation routes. The value of R is chosen such that the conductance varies from $G = 0$ when $tanh\,(k.s(t)) = -1$ (minimum) to $G = 2/R$ when $tanh\,(k.s(t)) = +1$ (maximum). The parameter k determines how the conductance varies from the lowest to the highest value. A higher value of k implies steeper is the movement from HRS to LRS and vice versa. The dynamics of state change in (4) is governed by varying the parameter τ. It is important that the state variable $s(t)$ is modeled as an internal branch voltage to overcome certain restrictions in the Verilog-A syntax [29].

The methodology used to model the I-V characteristics of the device is presented in the form of a flowchart in Fig. 4. At

TABLE I
PARAMETERS FOR POSITIVE AND NEGATIVE VOLTAGES

Parameter	$v(t) > 0$	$v(t) < 0$
R	150	60
k	6	50
τ	$5n$	$2n$

every time instant, the model considers the value of input voltage and the current state of the memristor. The model parameters were set according to Table I depending on the sign of the voltage. The current through the device at the current time was calculated as per (3), and the incremental change in state value was expressed by (4). Finally, this value was added to the current state and the state for the next time instant is obtained. The same steps were repeated for every time instant to mimic the switching behavior in the device.

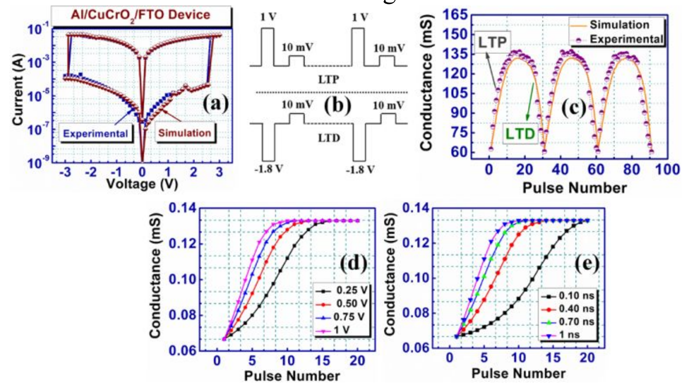

Fig. 5. (a) Experimental and simulated I-V characteristics of the Al/$CuCrO_2$/FTO device, (b) Voltage inputs to demonstrate LTP and LTD behavior in the devices, (c) Modulation of conductance of the memristor analogous to LTP and LTD, (d) The conductance variations corresponding to the input pulse amplitudes, and (e) Variation of conductance with pulse duration.

Hence, by considering appropriate values for the parameters in the above-mentioned model, the experimental I-V characteristics of the Al/$CuCrO_2$/FTO were repeated in simulation. For I-V characteristics, both the experimental and simulation results have been plotted and shown in Fig. 5(a). In order to obtain a good fit, the Verilog-A template [29] was modified and different parameters were considered for positive and negative voltages. The utilized parameters are presented in Table I. When a sine voltage input with amplitude of 3 V and a frequency of 50 MHz was considered, it is evident from Fig. 5(a) that the results of the model match the experimental results. Hence, the developed model can be used to portray the behavior of actual $CuCrO_2$ memristors in the simulation platform. It is noteworthy to mention that the state variable $s(t)$ is expected to be related to the number of oxygen vacancies in the device at any point, as the trapping and detrapping of electrons by these vacancies are responsible for the change of conductance in the device.

Biological synapses are a very important part of information processing in the nervous system. In simple terms, the synaptic weight increases with a set of excitatory inputs, while it decreases when the inputs are inhibitory in nature [25]. This change does not immediately disappear after the inputs are deactivated. Hence, these are termed as LTP and LTD, respectively. It was evident from both the experimental and

simulation results of the Al/$CuCrO_2$/FTO device that the conductance of the device gets increased with the increase in positive voltage, while a negative voltage results in a decrease in its conductance. As the device retains the resistance when no voltage was applied, it can potentially behave like a synapse. To demonstrate this behavior, a set of input pulses having a pulse width of 0.10 ns were considered. Pulses having a positive amplitude of +1 V were considered as excitatory inputs, while the amplitude of negative inhibitory inputs was chosen as −1.80 V as shown in Fig. 5(b). Each of these pulses was followed by a read phase, where the current corresponding to 10 mV input voltage was noted to calculate the conductance. When 15 excitatory input pulses were provided, the conductance changed from the HRS state to the LRS state corresponding to LTP. When this was followed by 15 inhibitory pulses, the device was brought back to HRS, which represents LTD. Two more such cycles, each with 15 excitatory and 15 inhibitory pulses were given to verify the repeatability of this phenomenon. These results (shown in Fig. 5(c)) demonstrate that $CuCrO_2$ devices are capable of mimicking LTP and LTD phenomenon, which makes them suitable for bio-inspired computing applications [3]. Interestingly, both the simulation and experimental results were well matched, therefore it validates each other.

It is noteworthy to mention that the choice of amplitude and width of the excitatory and inhibitory pulses chosen are arbitrary. By varying these parameters, the obtained response can be varied [36]. To demonstrate this process, we observe the conductance change when 20 pulses were given as input. In the first case, the pulse width was fixed at 100 ns and the amplitude was varied from 0.25 V to 1 V, with increments of 0.25 V. Fig. 5(d) shows the conductance change corresponding to these input pulses. As the pulse amplitude increases, the change in conductance value per pulse increases. Interestingly, this increase is not a linear one, as observed from the fact that the conductance values for a given pulse get closer as the voltage increases. This can be attributed to the non-linear I-V characteristics between 0 V to 1 V which was used to develop the simulation model (Fig. 5(a)). Another trend observed is that for all amplitudes, the conductance value saturates to about 13.30 mS. This value corresponds to the LRS with a maximum conductance value of $2/R$ in the developed model (R = 150, Table I). This shows that irrespective of the amplitude value, a sufficient number of input pulses can take the device to the LRS state. To study the effect of pulse width variations, the conductance change for 20 pulses having pulse widths of 10, 40, 70 and 100 ns was noted. For this study, the amplitude was fixed to 1 V. It is evident from Fig. 5(e) that the nature of conductance change is similar to the case of increasing amplitudes. For pulses having a smaller pulse width, more pulses were required to achieve the same conductance change as that corresponding to a pulse having a larger pulse width. Once again, the values saturate to the peak conductance value of 13.30 mS after a sufficient number of applied pulses. The same results were also mimicked through the simulation route, demonstrates its effectiveness for future neuromorphic computing.

In order to determine the non-volatile nature of the electronic synapse, it is important to evaluate whether the potentiation and depression is long term or of short duration.

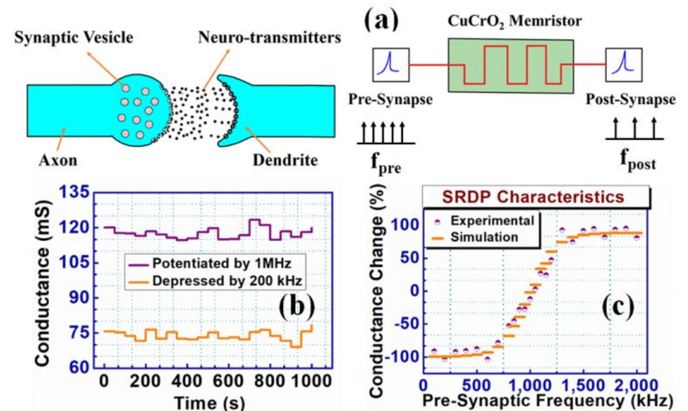

Fig. 6. (a) Schematic representation of a biological synapse and $CuCrO_2$ memristor emulating a synaptic role, (b) Synaptic conductance change with potentiation at 1000 kHz and depression by 200 kHz, and (c) SRDP characteristics of $CuCrO_2$ memristor.

A schematic of biological synapse and $CuCrO_2$ memristor emulating biological synapse with pre and post frequencies are shown in Fig. 6(a). From Fig. 6(b), it is evident that a change in conductance of 120 mS and 75 mS, observed at 1000 kHz and 200 kHz, respectively confirms the potentiation and depression of electronic synapses and this change was maintained over 1000 s confirming the change in the synaptic weight as long term [27]. Although LTP and LTD provide means to vary the conductance in $CuCrO_2$ memristive devices, it does not define exactly how this conductance change must be incorporated. Any biological synapse has two types of neurons connected to it viz. pre-synaptic and post-synaptic neurons. The difference in some property in the inputs from the pre-synaptic and post-synaptic neurons was believed to be the reason for synaptic weight variation [27], [37]. In our earlier work, we have utilized the STDP learning rule for biologically inspired computing applications [3]. However, STDP requires spikes that have to be engineered to a particular shape, which is a complex procedure. Another innovative learning rule is the SRDP, where the difference in the rate (or frequency) between pre- and post-synaptic pulses decides the magnitude and direction of weight change [27], [37]. Contrary to STDP, one only requires simple rectangular pulses to implement SRDP. Since the excitatory and inhibitory pulses orchestrate the LTP and LTD, respectively in $CuCrO_2$ memristor, one can use these pulses to establish the SRDP learning rule. It is expected that if there exist numerous excitatory inputs than inhibitory ones, then the conductance of the $CuCrO_2$ device gets increased, and vice versa. To verify this concept quantitatively, we consider post-synaptic pulses of width 0.10 ns and amplitude of +1.80 V. The frequency was fixed at 1000 kHz for this study. The pre-synaptic pulses had the same width as the post-synaptic ones, with an amplitude of +1 V. However, the frequency was varied from 100 kHz to 2000 kHz with small increments. For each frequency, the conductance was measured using a test voltage

1
2
3
4
5
6
7
8
9
10
11
12
13
14
15
16
17
18
19
20
21
22
23
24
25
26
27
28
29
30
31
32
33
34
35
36
37
38
39
40
41
42
43
44
45
46
47
48
49
50
51
52
53
54
55
56
57
58
59
60

of 10 mV before providing the inputs, and also after 10 μs of the simulation to evaluate the change in conductance. The percentage change in conductance was calculated as

$$\Delta G\ (\%) = \frac{G_f - G_i}{G_i} \times 100 \quad (5)$$

where G_i and G_f are the initial and final conductance values, respectively.

The results obtained are plotted in Fig. 6(c). As expected, the conductance decreased as the pre-synaptic frequency was reduced below 1000 kHz, which is the post-synaptic frequency. Nevertheless, for frequencies above 1000 kHz, the conductance increased. In addition, the magnitude of increment or decrement was higher when the difference between the pre- and post-synaptic input frequencies were increased. These results are significant enough to make ready the $CuCrO_2$ memristors for computing applications. By converting the input values into pulses having frequencies between 100 kHz and 2000 kHz, it was possible to vary the device conductance. The ability to change the state of the memristor can be further used for more efficient implementation of various applications [6]. The obtained results can also be compared with other memristors [27]. The simulation route was also adopted to accomplish the SRDP characteristics. From Fig. 6(c), it can be seen that both the experimental and simulation results were well matched, which possesses the validity of the proposed model for future generation neuromorphic computational systems.

IV. Conclusion

In summary, we have fabricated Al/$CuCrO_2$/FTO memristors and successfully demonstrated its impressive bipolar resistive switching behavior along with reliable retention (beyond 10^6 s). The proposed device was found to be highly enduring and maintained a high ON/OFF ratio throughout the measurement. To understand the device operational mechanism, a band-diagram was projected and it was found that a forming free process was responsible for HRS to LRS and LRS to HRS. Biological synaptic behavior was evidenced by engineering consecutive positive and negative pulses and the conductance change similar to LTP and LTD phenomenon were discovered in the proposed memristor. An attempt has been made to control the analog or synaptic behavior through pulse (pulse (amplitude and width) variations and the obtained results explicate its efficacy for bio-inspired neuromorphic systems. Since spiking neural network is beneficial to mimic the brain's capability at low power, finally, an innovative SRDP learning mechanism was realized to demonstrate the synaptic plasticity. This SRDP not only overcomes the shortcomings of the STDP mechanism but also reduces the hardware complexity as STDP requires spikes that have to be engineered to a particular shape, which is a complex procedure. In order to have better insights into the experimental observations, a similar Al/$CuCrO_2$/FTO memristor model has been developed through the simulation route, and both the experimental and simulation results were well matched, which opens up a new path for developing neuromorphic computing. One can further investigate the role of device area (by varying electrode diameters) and temperature (say from 300 to 450 K) on RS performances in $CuCrO_2$ memristor [38].

Acknowledgments

The authors sincerely acknowledge financial support from BRNS, DAE, Govt. of India (project No. 34/14/11/2017-BRNS/34286) and Science Foundation Ireland under grant no. 12/IA/1264 to carry out the research work. One of the authors Pavan is grateful to BRNS for his PhD fellowship support, whereas Pranab is thankful to Irish Research Council (IRC-GOIPD/2017/1275) for some financial supports. All the authors also appreciate BITS-Pilani Hyderabad Campus (including its cleanroom facilities) for providing all the technical supports.

References

[1] W. Banerjee, X. Xu, H. Lv, Q. Liu, S. Long, and M. Liu, "Complementary Switching in 3D Resistive Memory Array," Adv. Electron. Mater., vol. 3, no. 12, p. 1700287, Dec. 2017.

[2] P. K. R. Boppidi et al., "Unveiling the dual role of chemically synthesized copper doped zinc oxide for resistive switching applications," *Journal of Applied Physics*, vol. 124, no. 21, p. 214901, Dec. 2018.

[3] B. Suresh, P. K. R. Boppidi, B. V. V. S. N. Prabhakar Rao, S. Banerjee, and S. Kundu, "Realizing spike-timing dependent plasticity learning rule in Pt/Cu:ZnO/Nb:STO memristors for implementing single spike based denoising autoencoder," *J. Micromechanics Microengineering*, vol. 29, no. 8, p. 085006, Aug. 2019.

[4] W. Banerjee and H. Hwang, "Quantized Conduction Device with 6-Bit Storage Based on Electrically Controllable Break Junctions," Adv. Electron. Mater., vol. 5, no. 12, p. 1900744, Dec. 2019.

[5] W. Banerjee, Q. Liu, H. Lv, S. Long, and M. Liu, "Electronic imitation of behavioral and psychological synaptic activities using TiO:X/Al2O3-based memristor devices," Nanoscale, vol. 9, no. 38, pp. 14442–14450, Oct. 2017.

[6] M. Prezioso, F. Merrikh-Bayat, B. D. Hoskins, G. C. Adam, K. K. Likharev, and D. B. Strukov, "Training and operation of an integrated neuromorphic network based on metal-oxidememristors," *Nature*, vol. 521, no. 7550, pp. 61–64, May 2015.

[7] R. S. Williams, "What's Next?," *Computing in Science and Engineering*, vol. 19, no. 2, pp. 7–13, Mar. 2017.

[8] L. D. Bozano, B. W. Kean, V. R. Deline, J. R. Salem, and J. C. Scott, "Mechanism for bistability in organic memory elements," *Appl. Phys. Lett.*, vol. 84, no. 4, pp. 607–609, Jan. 2004.

[9] Z. B. Yan and J. M. Liu, "Resistance switching memory in perovskite oxides," *Ann. Phys. (N. Y).*, vol. 358, pp. 206–224, Jul. 2015.

[10] S. Yamamoto, T. Kitanaka, T. Miyashita, and M. Mitsuishi, "Resistive switching of organic-inorganic hybrid devices of conductive polymer and permeable ultra-thin SiO2 films," *Nanotechnology*, vol. 29, no. 26, p.26LT02, Apr. 2018.

[11] W. Banerjee, Q. Liu, and H. Hwang, "Engineering of defects in resistive random access memory devices," J. Appl. Phys., vol. 127, no. 5, p. 051101, Feb. 2020.

[12] J.-S. Huang *et al.*, "Bias Polarity-Induced Transformation of Point Contact Resistive Switching Memory from Single Transparent Conductive Metal Oxide Layer," *Adv. Electron. Mater.*, vol. 1, no. 8, p. 1500061, Aug. 2015.

[13] K. Fleischer, E. Norton, D. Mullarkey, D. Caffrey, and I. V. Shvets, "Quantifying the Performance of P-Type Transparent Conducting Oxides by Experimental Methods," Materials (Basel)., vol. 10, no. 9, p. 1019, Sep. 2017.

[14] E. Norton et al., "Bending stability of Cu0.4CrO2 - A transparent p-type conducting oxide for large area flexible electronics," AIP Adv.,

vol. 8, no. 8, p.085013, Aug. 2018.

[15] J. Crêpellière et al., “Transparent conductive CuCrO2 thin films deposited by pulsed injection metal organic chemical vapor deposition: Up-scalable process technology for an improved transparency/conductivity trade-off,” J. Mater. Chem. C, vol. 4, no. 19, pp. 4278–4287, 2016.

[16] M. Kubicek, S. Taibl, E. Navickas, H. Hutter, G. Fafilek, and J. Fleig, “Resistive states in strontium titanate thin films: Bias effects and mechanisms at high and low temperature,” *J. Electroceramics*, vol. 39, no. 1–4, pp. 197–209, Dec. 2017.

[17] L. Farrell, E. Norton, C. M. Smith, D. Caffrey, I. V. Shvets, and K. Fleischer, “Synthesis of nanocrystalline Cu deficient $CuCrO_2$-a high figure of merit p-type transparent semiconductor,” *J. Mater. Chem. C*, vol. 4, no. 1, pp. 126–134, 2015.

[18] D. Shin, J. S. Foord, R. G. Egdell, and A. Walsh, “Electronic structure of CuCrO2 thin films grown on Al 2O3(001) by oxygen plasma assisted molecular beam epitaxy,” *J. Appl. Phys*., vol. 112, no. 11, p.113718, Dec. 2012.

[19] C. Wang, W. He, Y. Tong, and R. Zhao, “ Investigation and Manipulation of Different Analog Behaviors of Memristor as Electronic Synapse for Neuromorphic Applications,” *Sci. Rep.*, vol. 6, Mar. 2016, Art. no. 22970.

[20] A. Sengupta, Z. Al Azim, X. Fong, and K. Roy, “Spin- orbit torque induced spike-timing dependent plasticity,” *Appl. Phys. Lett*., vol. 106, no. 9, p. 093704, Mar. 2015.

[21] J. M. Cruz-Albrecht, M. W. Yung, and N. Srinivasa, “Energy-efficient neuron, synapse and STDP integrated circuits,” *IEEE Trans. Biomed. Circuits Syst*., vol. 6, no. 3, pp. 246–256, 2012.

[22] S. Kim, Y. Abbas, Y. R. Jeon, A. S. Sokolov, B. Ku, and C. Choi, “Engineering synaptic characteristics of TaOx/HfO2 bi-layered resistive switching device,” *Nanotechnology*, vol. 29, no. 41, p.415204, Aug. 2018.

[23] M. Prezioso, F. Merrikh Bayat, B. Hoskins, K. Likharev, and D. Strukov, “Self-Adaptive Spike-Time-Dependent Plasticity of Metal-Oxide Memristors,” *Sci. Rep*., vol. 6, p. 21331, Feb. 2016.

[24] T. Serrano-Gotarredona, T. Masquelier, T. Prodromakis, G. Indiveri, and B. Linares-Barranco, “STDP and STDP variations with memristors for spiking neuromorphic learning systems,” *Front. Neurosci*., vol. 7, p. 2, Feb, 2013.

[25] G. Rachmuth, H. Z. Shouval, M. F. Bear, and C. S. Poon, “A biophysically-based neuromorphic model of spike rate- and timing-dependent plasticity,” *Proc. Natl. Acad. Sci. U. S. A.*, vol. 108, no. 49, Dec. 2011.

[26] T. Chang, S.-H. Jo, and W. Lu, “Short-Term Memory to Long-Term Memory Transition in a Nanoscale Memristor,” *ACS Nano*, vol. 5, no. 9, pp. 7669–7676, Sep. 2011.

[27] Y. Li *et al.*, “Activity-dependent synaptic plasticity of a chalcogenide electronic synapse for neuromorphic systems,” *Sci. Rep.*, vol. 4, p.4906, May 2014.

[28] Y. Wang, G. Wang, Y. Shen, and H. H.-C. Iu, “A Memristor Neural Network Using Synaptic Plasticity and Its Associative Memory,” *Circuits, Syst. Signal Process.*, pp. 1-16, Jan. 2020.

[29] T. Wang and J. Roychowdhury, “Well-Posed Models of Memristive Devices,” *arXiv preprint arXiv*:1605.04897, May 2016. Available: https://arxiv.org/abs/1605.04897

[30] F. Lin, C. Gao, X. Zhou, W. Shi, and A. Liu, “Magnetic, electrical and optical properties of p-type Fe-doped $CuCrO_2$ semiconductor thin films,” *J. Alloys Compd.*, vol. 581, pp. 502–507, 2013.

[31] T. Arnold *et al.*, “X-ray spectroscopic study of the electronic structure of $CuCrO_2$,” *Phys. Rev. B - Condens. Matter Mater. Phys.*, vol. 79, no. 7, p. 075102, Feb. 2009.

[32] B. Zhang, Y. Tian, J. X. Zhang, and W. Cai, “The role of oxygen vacancy in fluorine-doped SnO_2 films,” *Phys. B Condens. Matter*, vol. 406, no. 9, pp. 1822–1826, Apr. 2011.

[33] A. Korjenic and K. S. Raja, “Electrochemical stability of fluorine doped tin oxide (FTO) coating at different pH conditions,” *J. Electrochem. Soc.*, vol. 166, no. 6, pp. C169–C184, 2019.

[34] C. H. Li *et al.*, “Bipolar resistive switching with self-rectifying behaviors in p -type AgCr1- $xMgxO_2$ thin films,” *J. Appl. Phys.*, vol. 126, no. 8, p. 085702, Aug. 2019.

[35] J. W. Han and M. Meyyappan, “Copper oxide resistive switching memory for e-textile,” *AIP Adv.*, vol. 1, no. 3, p.032162, 2011.

[36] S. Kim, H. Kim, S. Hwang, M.-H. Kim, Y.-F. Chang, and B.-G. Park, "Analog Synaptic Behaviour of a Silicon Nitride Memristor," *ACS Appl. Mater. Interfaces,* vol. 9, no. 46, p. 40420, Nov. 2017.

[37] W. He et al., “Enabling an integrated rate-temporal learning scheme on memristor,” *Sci. Rep.*, vol. 4, p.4755, Apr. 2014.

[38] N. Singh and D. Kaur, “Origin of tri-state resistive switching characteristics in SiCN thin films for high-temperature ReRAM applications,” *Appl. Phys. Lett*., vol. 113, p.162103, Oct. 2018.

1
2
3
4
5
6
7
8
9
10
11
12
13
14
15
16
17
18
19
20
21
22
23
24
25
26
27
28
29
30
31
32
33
34
35
36
37
38
39
40
41
42
43
44
45
46
47
48
49
50
51
52
53
54
55
56
57
58
59
60